Asian Journal of Chemistry; Vol. 38, No. 1 (2026), 89-96
ASIAN JOURNAL OF CHEMISTRY
https://doi.org/10.14233/ajchem.2026.34809

Impact of Annealing Temperature on Structural Variations, Optical and Magnetic Behaviour of CdO/$FePO_4$ Nanophosphors

S.K. KHAJAMUSWAREEN[1,*], G. SREEDEVI[2], K. VENKATARAO[3], K. SRINIVAS[4] and V. JAYALAKSHMI[5]

[1]Department of Physics, P.B. Siddhartha College of Arts & Science, Vijayawada-520010, India
[2]Department of Physics, P.V.P. Siddhartha Institute of Technology, Vijayawada-520007, India
[3]Department of Physics, Government Institute of Textile Technology, Guntur-522005, India
[4]Department of Physics, Kakatiya Institute of Technology and Science, Warangal-506015, India
[5]Department of Physics, National Institute of Technology, Warangal-506004, India

*Corresponding author: E-mail: khajamuswareen@gmail.com

Received: 1 September 2025 *Accepted*: 6 November 2025 *Published online*: 31 December 2025 AJC-22226

In present investigation, cadmium oxide-iron phosphate (CdO-$FePO_4$) nanophosphors were prepared by chemical precipitation method. To understand the internal structural, optical, luminescence variations with effect of annealing temperature, the prepared samples are annealed at 200 ºC and 400 ºC for 8 h. X-ray diffractometry (XRD) analysis of the synthesized powder nanophosphors reveals the presence of an amorphous $FePO_4$ phase along with a crystalline cubic CdO phase at a calcination temperature of 200 ºC. Upon increasing the annealing temperature to 400 ºC, the amorphous $FePO_4$ transitions into a hexagonal crystalline phase, while the CdO phase remains unchanged in its cubic structure. The average crystallite size, lattice strain and dislocation density were also calculated to further characterize the material structure. Field emission scanning electron microscopy (FE-SEM) images show a heterostructured morphology consisting of rectangular flakes surrounded by hexagonal spheres. As the annealing temperature increases, the size of the rectangular flakes decreases and the hexagonal spheres develop into a network structure, forming narrow rod-like morphologies that are distributed over the surface. Energy dispersive X-ray spectroscopy (EDAX) confirms the presence of all requisite elements in the prepared nanophosphors. Fourier transform infrared (FT-IR) spectroscopy indicates vibrational modes corresponding to regular PO_4 tetrahedra and metallic Cd-O bonding. With increasing temperature, the energy band gap decreases, it confirms the semiconducting behaviour of the CdO-$FePO_4$ nanocomposites.

Keywords: Cadmium oxide, Iron phosphate, Chemical precipitation, Energy band gap, Semiconducting nanocomposites.

INTRODUCTION

In recent years, the synthesis of nanocrystalline metal oxide materials has gained significant attention and emerged at the forefront of research, owing to their distinctive properties and broad technological applications [1-4]. Among these, semiconductor metal-oxide nanoparticles have received particular focus due to their tunable band gaps, high surface-to-volume ratios, and versatile physicochemical characteristics, which make them highly suitable for applications in sensors, electronics, biomedical devices and advanced material technologies [5].

In recent trends, nanohybrid or nanocomposite materials have become increasingly important in the development of advanced phosphors due to their ability to combine the advantages of multiple constituent phases, thereby overcoming limitations of individual materials [6-9]. In phosphor technology, composite structures typically consist of a luminescent phase of phosphates integrated with supportive matrices like polymers, metal oxides or carbon-based materials. This combination leads to synergistic effects that enhance structural, thermal and optical performance [10,11].

Cadmium oxide (CdO) plays a significant role in the development and enhancement of luminescent phosphor materials. As a wide bandgap n-type semiconductor, CdO exhibits favourable optical and electronic properties, including high electrical conductivity, good thermal stability and a direct bandgap typically ranging from 2.2 to 2.5 eV. When incorporated into phosphor systems, CdO acts as a host matrix or a modifying agent that can influence the structural, morpholo-

gical and luminescent characteristics of the resulting material [12,13]. CdO can improve crystallinity and reduce non-radiative recombination centers, thereby increasing the quantum efficiency and stability of the phosphor material [14,15]. Similarly, iron(III) phosphate ($FePO_4$) has also gained increasing attention as a functional component in phosphor materials due to its chemical stability, environmental friendliness and structural versatility [16,17]. Nano-$FePO_4$ serves as an effective host matrix or co-dopant in the development of luminescent phosphors, particularly in applications where non-toxic, earth-abundant and cost-effective materials [18,19].

In this work, the synthesis of CdO-$FePO_4$ nanocomposite as nanophosphors is carried out by chemical precipitation method and systematically investigate the impact of annealing temperature on the structural, optical, morphological, and magnetic properties.

EXPERIMENTAL

Analytical grade chemicals *viz*. cadmium nitrate tetrahydrate ($Cd(NO_3)_2{\cdot}4H_2O$, ≥99%), iron(III) nitrate nonahydrate ($Fe(NO_3)_2{\cdot}9H_2O$, ≥99%) and trisodium phosphate (Na_3PO_4, ≥98%) were used as primary precursors for the synthesis of CdO-$FePO_4$ nanocomposites and procured from Sigma-Aldrich, USA. Analytical-grade NaOH solution was employed as the precipitating agent to adjust the pH during synthesis. Deionized (DI) water was used throughout all solution preparations and washing steps to ensure contaminant free processing, while absolute ethanol (≥99%) was used for rinsing and to promote drying and prevent agglomeration of the obtained precipitates. All chemicals and solvents were used as received without any further purification.

Characterization: X-ray diffraction (XRD) was performed on a PANalytical X'Pert PRO diffractometer using Cu*K*α radiation (λ = 1.5406 Å) over a 2θ range of 20-90º to determine phase composition, lattice parameters, crystallite size, strain and dislocation density. Surface morphology was analyzed using a TESCAN VEGA3 LMU SEM operated at 15 kV and particle size distribution was further evaluated using ImageJ software. Elemental composition and purity were confirmed through EDAX attached to the same SEM instrument. FTIR spectroscopy (4000-400 cm^{-1}) was used to identify the functional groups and monitor structural changes with temperature, whereas optical properties were studied by UV-Vis diffuse reflectance spectroscopy using a Specord 210 Plus spectrophotometer in the 300-1000 nm range, with band gaps estimated *via* the Kubelka-Munk function. Magnetic behaviour was assessed using a vibrating sample magnetometer (VSM) by recording M–H hysteresis loops to extract saturation magnetization, remanence and coercivity.

Synthesis of CdO-$FePO_4$ nanophosphors: To synthesize CdO-$FePO_4$ nanophosphors, 2.3642 g of $Cd(NO_3)_2{\cdot}4H_2O$ was dissolved in 20 mL of distilled water and magnetically stirred for 15 min. In a separate beaker, 2.4186 g of $Fe(NO_3)_2{\cdot}9H_2O$ and 1.6394 g of Na_3PO_4 were dissolved in 20 mL of distilled water. The resulting solution was then added dropwise to the cadmium nitrate solution under continuous stirring. The combined mixture was magnetically stirred at 700 rpm for 24 h, promoting homogeneous mixing and particle-size reduction through continuous internal collisions. A dark brown precipitate gradually formed during this process. The precipitate was collected and washed several times with distilled water to remove residual impurities. The final product was dried and then annealed at two different temperatures, 200 ºC and 400 ºC, to obtain CdO-$FePO_4$ nanophosphors with controlled crystallinity and phase formation.

RESULTS AND DISCUSSION

XRD analysis: The XRD pattern of CdO-$FePO_4$@200 ºC sample displays broad and intense peaks, suggesting the presence of both crystalline and amorphous phases. The major peaks matched well with the standard JCPDS card no. 01-075-0591 for CdO (Fig. 1a). However, $FePO_4$ peaks are not distinctly visible indicating that $FePO_4$ is either poorly crystallized or present in minute amounts at this temperature. The broad hump in the background baseline also suggests amorphous content or poor particle ordering, typical of low-temperature synthesis. With increasing of annealing temperature, CdO-$FePO_4$ @400 ºC sample (Fig. 1b) shows sharper and more intense diffraction peaks indicating enhanced crystallinity and well-formed crystal structures due to higher calcination temperature and gradually amorphous $FePO_4$ transformed into hexagonal $FePO_4$ after annealing at 400 ºC as supported with JCPDS card nos. 00-017-0837 for $FePO_4$ [20-24]. The peaks corresponding to CdO also remain consistent with the CdO standard (JCPDS card no. 01-075-0591), confirming phase stability upon heating. The disappearance of a broad amorphous background and the increased number of well-resolved peaks phases purity and crystalline domain growth.

The relevant lattice parameters, unit cell volume and symmetry axes of prepared samples derived from the XRD spectra are listed in Table-1. These values are well correlated with the conventional JCPDS values. The average crystallite size (D), lattice strain (ε), dislocation density (δ) values of the prepared CdO-$FePO_4$ nanophosphors were deduced using

TABLE-1
PARAMETERS CALCULATED FROM XRD SPECTRA

Sample name	2θ (º)	Crystallite Size, D (nm)	Strain $\varepsilon \times 10^{-4}$	Dislocation density (δ) (lines/m^2)	Lattice parameter (Å)	Unit cell volume, V $(Å)^3$	Percentage of crystallinity (%)
CdOFePO$_4$ (200 ºC)	33.02	20.39	59.13	2.40×10^{15}	CdO: a=b=c=4.691	CdO: 103.210	36.71
CdOFePO$_4$ (400 ºC)	33.01	29.12	53.8	1.173×10^{15}	CdO: a=b=c=4.689 FePO$_4$: a=b=5.033, c=5.595	CdO: 103.159 FePO$_4$: 122.777	88.96

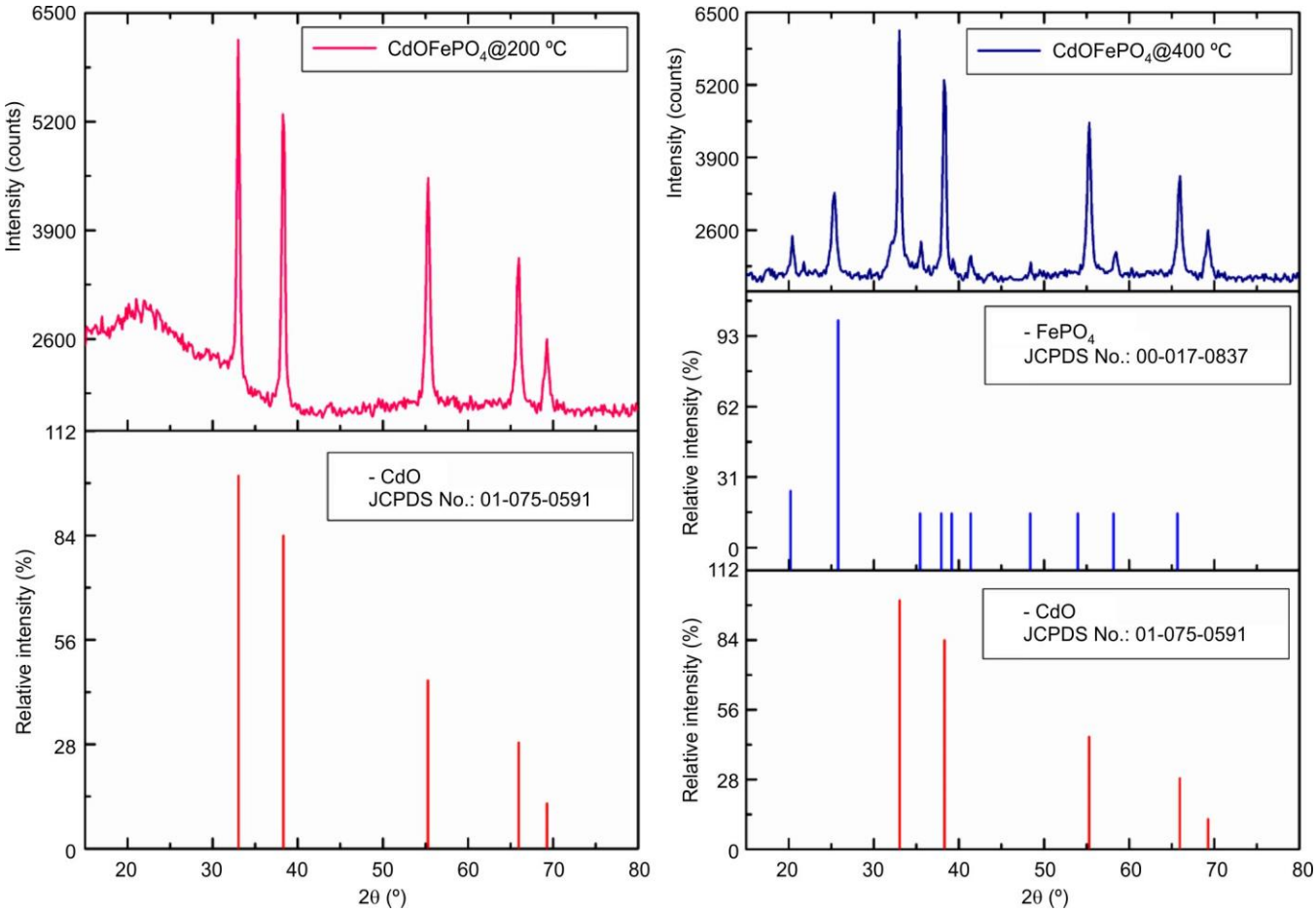

Fig. 1. XRD pattern of CdO-$FePO_4$ nanophosphors annealed at 200 ºC and 400 ºC

Debye-Scherrer's, Stokes-Wilson and Williamson-Smallman equations by using eqns. 1-3, respectively [25-27].

$$D = \frac{0.89\lambda}{\beta \cos\theta} \quad (1)$$

$$\varepsilon = \frac{\beta}{4\tan\theta} \quad (2)$$

$$\delta = \frac{1}{D^2} \quad (3)$$

where λ = incident X-ray wavelength (1.5406 Å), β = FWHM (full width half maxima) of most prominent peak in radians and θ = Bragg's diffraction angle. The resultant values of D, ε and δ for CdO-$FePO_4$ nanophosphors at two different temperatures are also shown in Table-1. The variation in crystallite size and lattice parameter at two different temperatures can be described on the basis of synergic effect due to thermal excitation of the nanoparticles [28]. The observed increase in strain and dislocation density reflects the lattice distortions induced in the nanophosphors as a result of the change in annealing temperature.

The determination of the percentage crystallinity or crystallinity index, is of significant interest due to it direct influences the optoelectronic properties of the material and provides insight into the degree of structural purity. The relative percentage crystallinity of the samples was calculated using eqn. 4, which evaluates the ratio of the total area of crystalline peaks to the total area under the XRD diffractogram [29,30].

$$\text{Crystallinity } (\%) = \frac{I_c}{I_c + I_a} \quad (4)$$

Here I_c is the total intensity of the crystalline peaks; I_a is the total intensity of the amorphous peaks.

The determined values of relative percentage crystallinity of CdO-$FePO_4$ nanophosphors annealed at 200 and 400 ºC are also given in Table-1. The XRD analysis confirms that calcination temperature plays a vital role in the structural evolution of the CdO-$FePO_4$ nanophosphors. The sample prepared at 400 ºC exhibits superior crystallinity, well-defined CdO and $FePO_4$ phases and greater structural order compared to the 200 ºC sample. These features are crucial for optimizing the properties in applications like phosphors, catalysts and electronic materials.

Morphological studies: The SEM micrograph images of prepared samples are shown in Fig. 2. The microstructures of CdO-$FePO_4$ ~200 ºC shows high surface roughness with a loosely packed, irregular morphology. Particles appear to be fine, highly agglomerated and less defined, indicating incomplete crystallization. The presence of many smaller grains with uneven shapes suggests that the material is still undergoing growth and phase development. The observed texture is typical of materials calcined at lower temperatures, where volatile

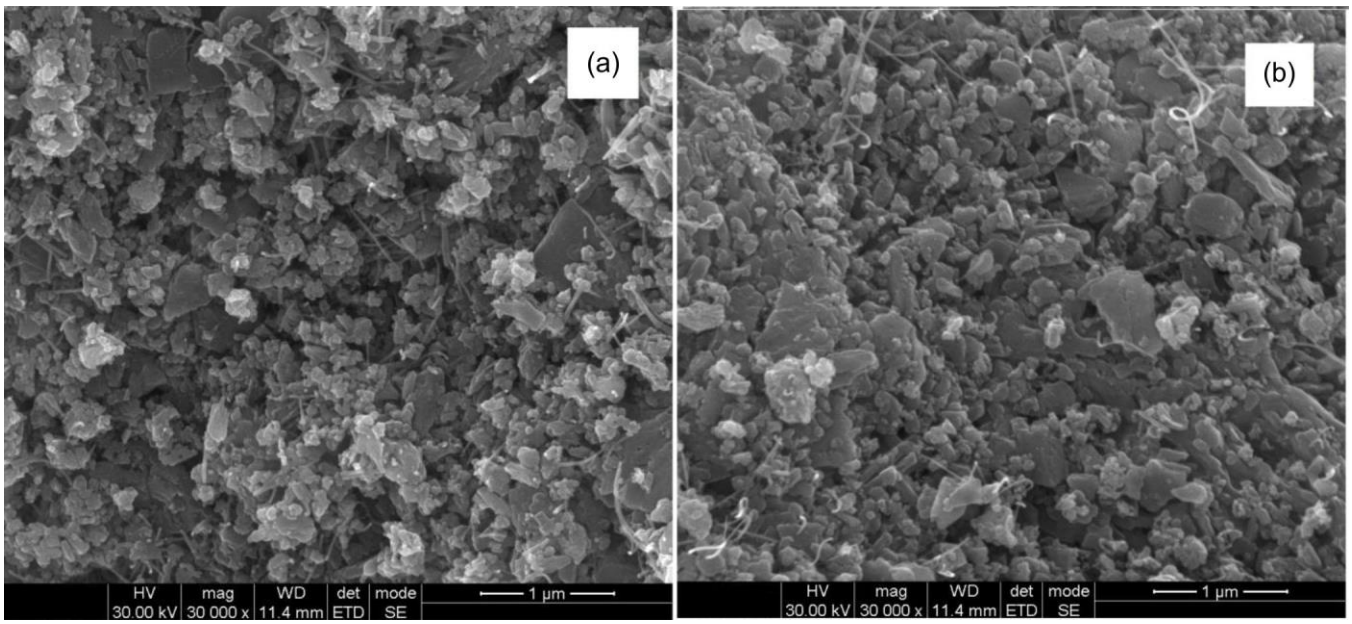

Fig. 2. SEM micrographs of CdO-$FePO_4$ nanophosphors annealed at (a) 200 ºC and (b) 400 ºC

residues (*e.g.* hydroxyls, nitrates) may not be fully eliminated, leading to porous and disordered morphology. The CdO-$FePO_4$ ~400 ºC sample exhibits a more densely packed and consolidated structure. The particles appear larger and more well-defined, exhibiting distinct plate-like and crystalline features. The observed reduction in porosity and increase in grain size indicate grain growth and sintering, facilitated by the higher calcination temperature. The relatively uniform morphology reflects enhanced crystallinity and improved phase formation consistent with the thermal decomposition of residual precursors and the formation of stable CdO-$FePO_4$ phases

By using Image-J software, particle size distribution histograms are drawn for synthesized CdO-$FePO_4$ samples at two different temperatures 200 ºC and 400 ºC are shown in Fig. 3. The synthetic temperature significantly impacts particle size distribution of CdO-$FePO_4$ nanophosphors. Lower temperatures yield more non-uniform and smaller particles, while higher temperatures lead to broader and more varied particle sizes due to increased grain growth or agglomeration effects. The average particle sizes, determined from histogram of measured diameters and widths of spheres and rods (Fig. 3), are 34.98 nm and 32.60 nm for samples annealed at 200 ºC and 400 ºC, respectively. These values are larger than the corresponding crystallite sizes reported in Table-1, suggesting that each particle is composed of multiple crystallites rather than a single crystalline domain [31].

Fig. 4 represents the EDAX spectrum of CdO-$FePO_4$ nanophosphors annealed at 200 and 400 ºC. The results show the presence of Cd, O, Fe and P elements without any other impurity, showing the high pure nature of the prepared nanophosphors.

FTIR spectral studies: FTIR spectra of the CdO-$FePO_4$ nanophosphors annealed at 200 ºC and 400 ºC are shown in Fig. 5. The FTIR spectra of CdO-$FePO_4$ nanophosphors calcined at 200 ºC and 400 ºC exhibit significant differences in band intensity and sharpness indicating temperature dependent structural and bonding changes.

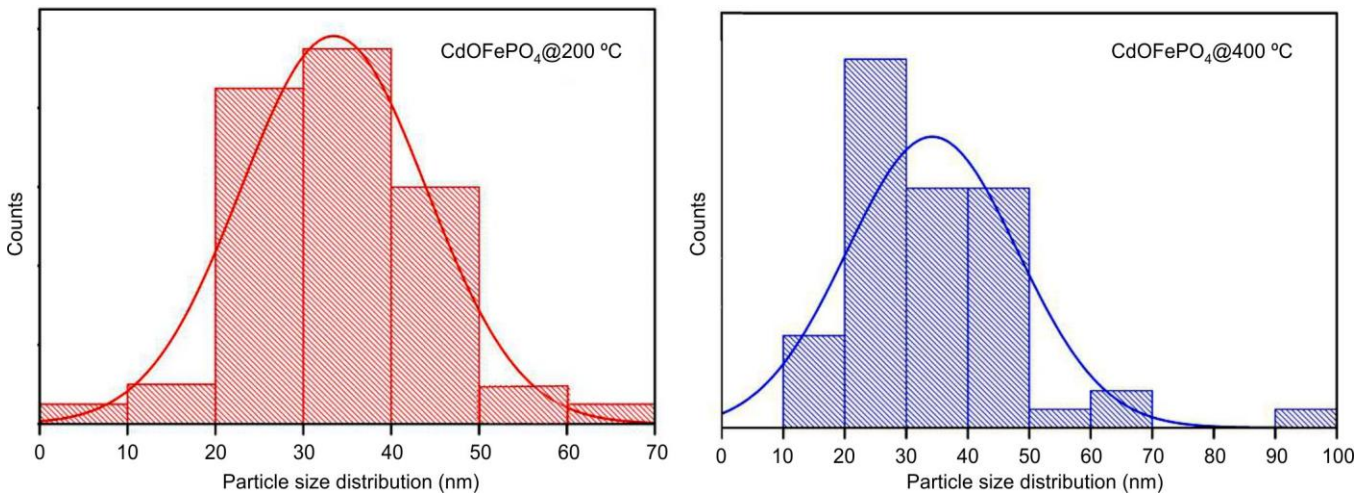

Fig. 3. Size distribution plots of CdO-$FePO_4$ nanophosphors annealed at 200 and 400 ºC

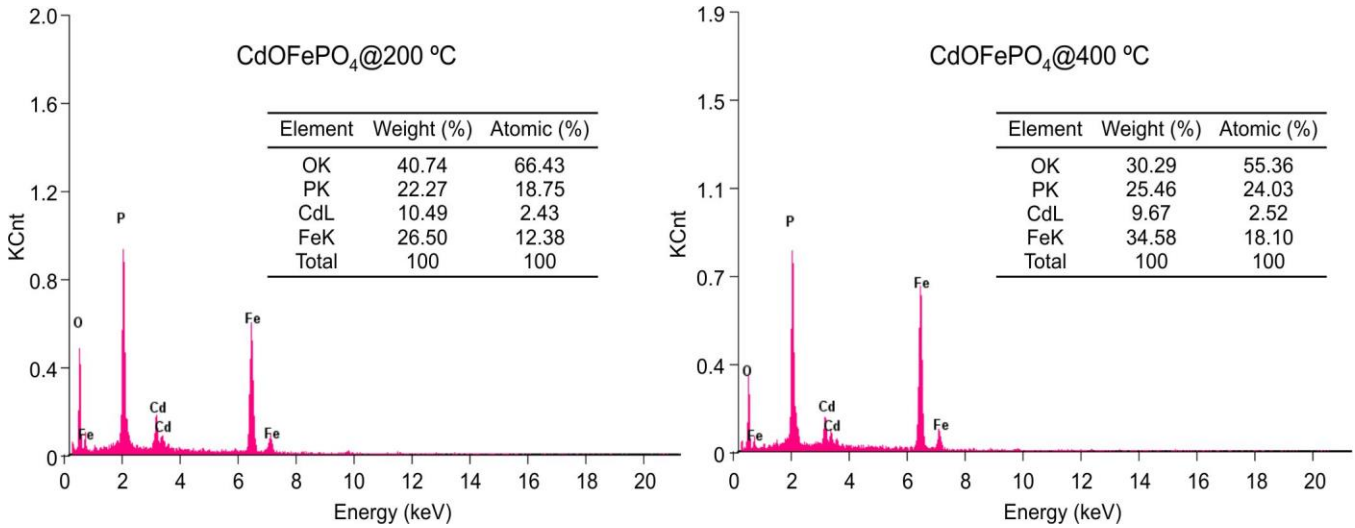

Fig. 4. EDAX patterns of CdO-$FePO_4$ nanophosphors annealed at 200 ºC and 400 ºC

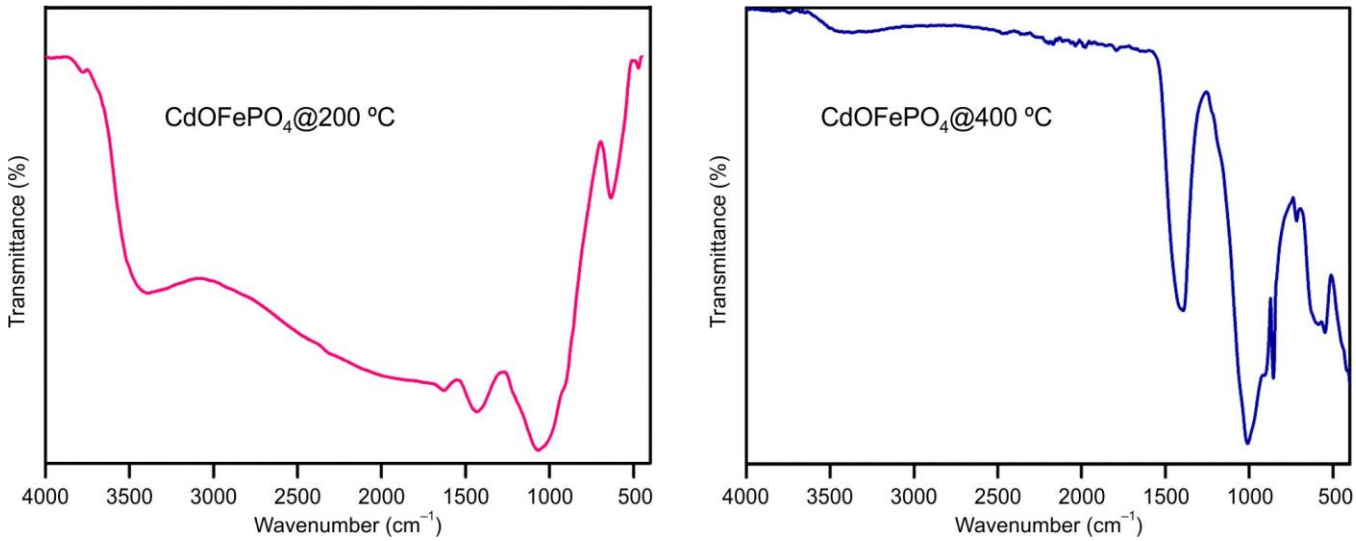

Fig. 5. FT-IR spectra of CdO-$FePO_4$ nanophosphors annealed at 200 ºC and 400 ºC

For 200 ºC sample, a broad and intense absorption band appears around ~3400 cm^{-1}, corresponding to O–H stretching vibrations from physically adsorbed water or residual hydroxyl groups. This band is significantly weakened in the 400 ºC sample indicating the removal of moisture and hydroxyl species due to high-temperature-induced dehydration or condensation. Moreover, a band near 1630 cm^{-1} in the 200 °C spectrum is assigned to H–O–H bending vibrations, confirming the presence of adsorbed water. This feature is diminished or absent in the 400 ºC sample, reflecting improved water removal upon thermal treatment.

Both spectra show strong bands in the 1000-500 cm^{-1} region, attributed to P–O stretching and O–P–O bending vibrations, characteristic of $FePO_4$ or phosphate networks. These bands become sharper and better defined in the 400 º sample, indicating enhanced crystallinity and structural ordering of the phosphate framework. Bands below 700 cm^{-1} correspond to Cd–O and Fe–O bond vibrations, and the increased intensity and sharpness of these bands in the 400 ºC sample suggest improved formation of M-O linkages and higher phase purity.

Overall, the 200 ºC sample exhibits broader, less defined peaks with prominent O–H and H–O–H signals, indicative of structural water and incomplete crystallization. In contrast, the 400 ºC sample shows sharper, well-resolved bands with reduced water-related absorptions, confirming enhanced crystallinity, stronger bond formation, and fewer defects [32,33]. These FTIR results corroborate the local structural environments and bonding in the CdO-$FePO_4$ nanophosphors. The characteristic peak positions and shifts for samples annealed at 200 ºC and 400 ºC are summarized in Table-2.

DRS study: The optical bang gap values of CdO-$FePO_4$ nanophosphors were deduced from Kubelka-Munk (K-M) function using eqn. 5 [34]:

$$F(R) = \frac{(1-R)^2}{2R} \tag{5}$$

where F(R) is a K-M function; R is the reflectivity of sample. The above equation can be rewritten with the equation relating band gap (E_g) as follows [27]:

$$(\alpha h\nu) = F(R)h\nu = A(h\nu - E_g)^n \tag{6}$$

TABLE-2
ASSIGNMENT OF VARIOUS BAND POSITIONS AND THEIR CORRESPONDING FREQUENCIES IN IR SPECTRA OF CdO-$FePO_4$ NANOPHOSPHORS

Position of bands (cm^{-1})		Assignment
$CdOFePO_4$ (200 ºC)	$CdOFePO_4$ (400 ºC)	
3424	3420	-OH stretching
1631	–	-OH bending
1431	1400	$-CH_2$ bending
1062	1010	Anti-symmetric stretching of PO_4^{3-}: $F_2^{(2)}$
–	855, 718	P–O bond symmetric stretching vibrations: A_1
634	546	O–P–O bending vibrations: $F_2^{(1)}$
470	431	Metallic bonding of CdO

where the values of n = 1/2, 2, 3/2 and 3 indicate allowed direct, allowed indirect, direct forbidden and indirect forbidden transitions, respectively [35]. The band gap values for the prepared samples were extrapolated from the graph drawn between $(F(R)h\nu)^2$ *versus* energy (hν) (Fig. 6).

The $CdOFePO_4$ sample annealed at 200 ºC exhibits a band gap of 2.26 eV, while the sample annealed at 400 ºC shows an increased band gap of 3.0 eV. The lower band gap at 200 ºC is attributed to a higher density of defect states and the presence of localized electronic states near the band edges, typically associated with amorphous or poorly crystallized phases. In contrast, the higher band gap observed at 400 ºC indicates improved crystallinity and reduced defect density, consistent with the XRD analysis. This increase in band gap with annealing temperature reflects a reduction in the mid-gap states and enhanced phase purity, leading to a blue shift in the absorption edge. This shift also indicates controlled tuning of optical properties *via* synthesis conditions. Consequently, the 400 ºC sample is more suitable for UV-light-driven applications such as UV sensors and photo-electrochemical devices.

Magnetic properties: From the M-H loops of CdO-$FePO_4$ annealed at 200 ºC exhibits saturation magnetization, remnant magnetization and the coercivity were found to be 0.002405 emu/g, 0.0003352 emu/g, 628 Oe, respectively. This sample shows the reasonably high magnetization under strong applied fields. A moderate coercive field, implying the material has some resistance to demagnetization. This behaviour suggest it act as semi-hard magnet suitable for memory applications or magnetic sensors. Small residual magnetization occurs when the field is removed it indicates the material can retain some magnetism but not strongly. The magnetic hysteresis loop shown in Fig. 7a exhibits slight asymmetry, which may arise from anisotropic magnetic domains or sample imperfections. The relatively low saturation magnetization is attributed to the nanostructured nature of the particles and the mixed oxide composition of the CdO-$FePO_4$ nanophosphors.

The CdO-$FePO_4$ sample annealed at 400 ºC exhibits saturation magnetization, remnant magnetization and the coercivity were found to be 0.002731 emu/g, 0.000449 emu/g, 1155 Oe, respectively. With increasing annealing temperature, all the magnetic parameters show an increase, indicating that the magnetic domains become more systematically aligned and exhibit enhanced resistance to demagnetization. The Hc value increases with particle size, which is possibly due to domain wall pinning or reduced surface effects. The EDS analysis reveals that CdO-$FePO_4$@400 ºC contains a higher Fe content (~34.6 wt.%) compared to the 200 ºC sample indicated that Fe incorporation increases with annealing temperature. This enhanced Fe content correlates with the observed improvement in the magnetic properties at higher temperatures.

Conclusion

In conclusion, CdO-$FePO_4$ nanophosphors were successfully synthesized using a simple and cost-effective chemical precipitation method. The annealing process played a key role in enhancing the crystalline quality of the nanophosphors. X-ray diffraction analysis confirmed the presence of two distinct phases and demonstrated that the crystallinity of the samples improved with increasing annealing temperature The formation of nanospheres with rod like association around them is shown by SEM. Elementary mapping through EDAX spectrum confirmed that the initial precursors converted into final material in accordance to their stoichiometric ratios. Peaks related to Cd–O and P bonds were observed in the FT-

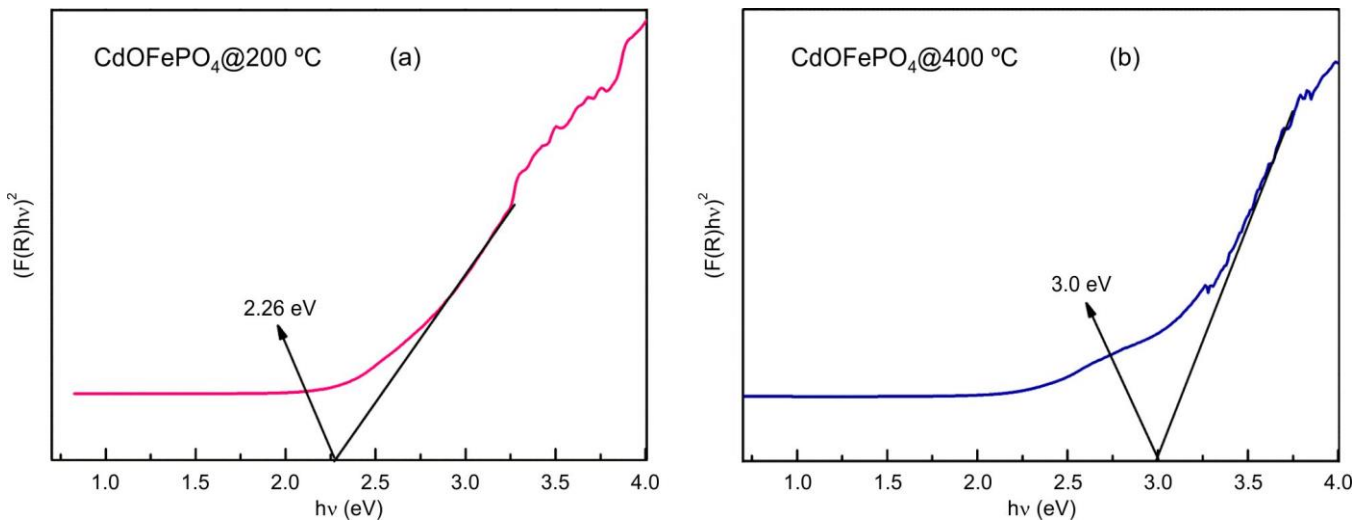

Fig. 6. The optical band gap plots of CdO-$FePO_4$ nanophosphors annealed at 200 ºC (a) and 400 ºC (b)

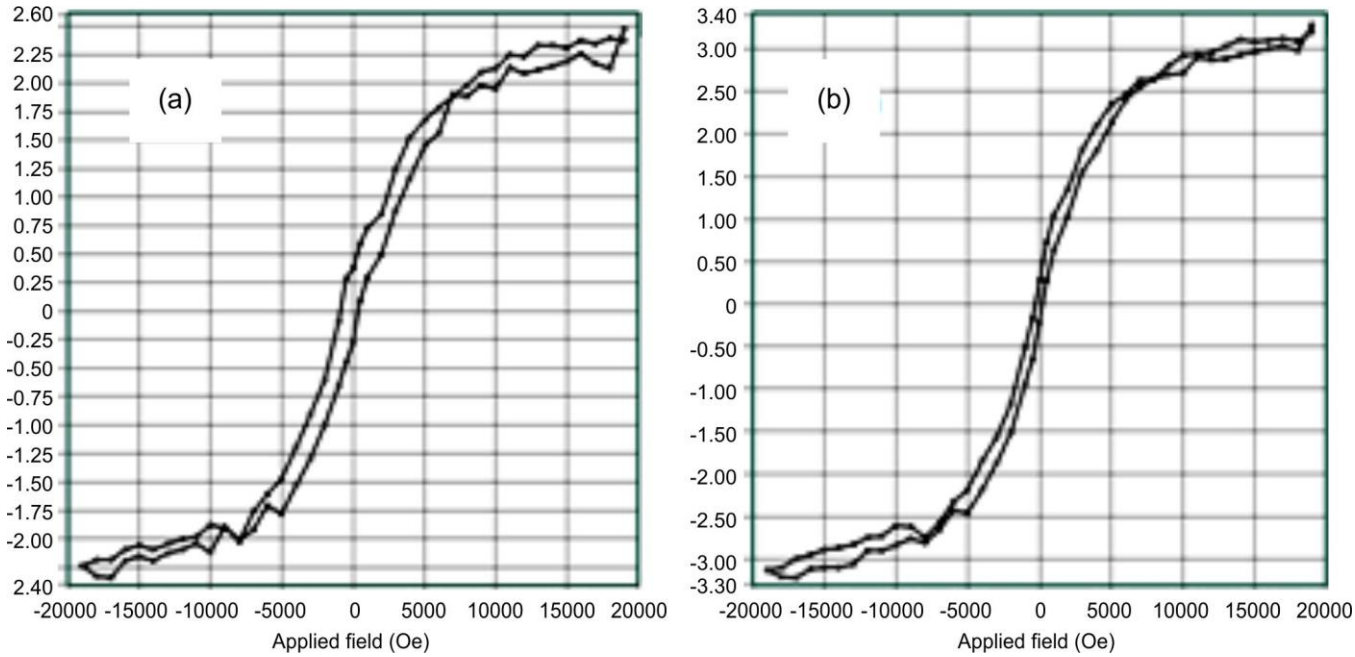

Fig. 7. M-H curve of CdO-$FePO_4$ nanophosphors (a) 200 ºC and (b) 400 ºC

IR spectrum. The indirect band gap calculated from diffused reflectance spectra varied as 2.26 eV and 3.0 eV for annealing temperatures at 200 ºC and 400 ºC. This means that the prepared nanophosphors can efficiently absorb visible light photons, which is crucial for many photocatalytic reactions.

ACKNOWLEDGEMENTS

One of the authors, SKM, thanks Siddhartha Academy of General & Technical Education (SAGTE), Vijayawada, India for sanctioning the seed money grant (O.C. No. 37/2023/ PBSC/2022-2023, Dt: 05-01-2023) to carry this research.

CONFLICT OF INTEREST

The authors declare that there is no conflict of interests regarding the publication of this article.

DECLARATION OF AI-ASSISTED TECHNOLOGIES

During the preparation of this manuscript, the authors used an AI-assisted tool(s) to improve the language. The authors reviewed and edited the content and take full responsibility for the published work.

REFERENCES

1. Y. Mao and S.K. Gupta, *Nanomaterials*, **12**, 4340 (2022); https://doi.org/10.3390/nano12234340
2. Y. Mao and S.K. Gupta, *Green Chem.*, **26**, 7579 (2024); https://doi.org/10.1039/D4GC01870B
3. K. Kamata, T. Aihara, and K. Wachi, *Chem. Commun.*, **60**, 11483 (2024); https://doi.org/10.1039/D4CC03233K
4. R. Ullah, M. Siraj, F. Zarshan, B.A. Abbasi, T. Yaseen, A. Waris and J. Iqbal, *Rev. Inorg. Chem.*, **45**, 411 (2025); https://doi.org/10.1515/revic-2024-0031
5. R. Nallendran, G. Selvan and A.R. Balu, *Mater. Sci. Pol.*, **37**, 100 (2019); https://doi.org/10.2478/msp-2019-0012
6. R. Kirana, N. Kamath, M.I. Sayyed, A.H. Almuqrin and S.D. Kamath, *RSC Adv.*, **15**, 20040 (2025); https://doi.org/10.1039/D5RA03126E
7. M. Rakshita, A.A. Sharma, P.P. Pradhan, K.A.K.D. Prasad, M. Srinivas and D. Haranath, *Mater. Adv.*, **6**, 3203 (2025); https://doi.org/10.1039/D5MA00117J
8. S. Alamdari, M.J. Tafreshi and M.S. Ghamsari, *J. Semicond.*, **43**, 122301 (2022); https://doi.org/10.1088/1674-4926/43/12/122301
9. S. Alamdari, M. Mansourian and M. Ghamsari, *Curr. Nanomater.*, **9**, 279 (2024); https://doi.org/10.2174/2405461508666230829102228
10. L. Mebarki, B. Kahouadji, A. Zoukel, L. Benharrat, J. Prakash, S. Ouhenia, A. Souici, M. Delaey, L. Guerbous, D. Poelman and H.C. Swart, *J. Fluoresc.*, **35**, 5391 (2025); https://doi.org/10.1007/s10895-024-03915-2
11. Y. Sun, Y. Wang, W. Chen, Q. Jiang, D. Chen, G. Dong and Z. Xia, *Nat. Commun.*, **15**, 1033 (2024); https://doi.org/10.1038/s41467-024-45293-0
12. C. Bhukkal, M. Chauhan and R. Ahlawat, *Phys. B: Condens. Matter*., **582**, 411973 (2020); https://doi.org/10.1016/j.physb.2019.411973
13. A.E. El-Hadary, H.H. El-Feky, A. El-Qanni, I.M. Nassar and M.Y. Nassar, *Asian J. Chem. Sci.*, **13**, 24 (2023); https://doi.org/10.9734/ajocs/2023/v13i1230
14. R.J. Stella, G.T. Rao, V.P. Manjari, B. Babu, Ch. R. Krishna and R.V.S.S.N. Ravikumar, *J. Alloys Compd.*, **628**, 39 (2015); https://doi.org/10.1016/j.jallcom.2014.11.201
15. G. Singh and M.S. Chauhan, *Mater. Chem. Phys.*, **308**, 128302 (2023); https://doi.org/10.1016/j.matchemphys.2023.128302
16. M. Poienar, M.J. Gutmann, G.L. Pascut, V. Petříček, G. Stenning, P. Vlazan, P. Sfirloaga, C. Paulmann, M. Tolkiehn, P. Manuel and P. Veber, *Materials*, **15**, 8059 (2022); https://doi.org/10.3390/ma15228059
17. S.I.A. Shah, W. Ahmad, M. Anwar, R. Shah, J.A. Khan, N.S. Shah, A. Al-Anazi and C. Han, *Appl. Catal. O: Open*, **203**, 207049 (2025); https://doi.org/10.1016/j.apcato.2025.207049
18. V.S. Saji and H.-K. Song, *J. Nanosci. Nanotechnol.*, **15**, 734 (2015); https://doi.org/10.1166/jnn.2015.9173
19. Y. Lu, T. Zhang, Y. Liu and G. Luo, *Chem. Eng. J.*, **210**, 18 (2012); https://doi.org/10.1016/j.cej.2012.08.077
20. Y. Song, S. Yang, P.Y. Zavalij and M.S. Whittingham, *Mater. Res. Bull.*, **37**, 1249 (2002); https://doi.org/10.1016/S0025-5408(02)00771-7

21. B. Lee, C. Kim, Y. Park, T.G. Kim and B. Park, *Electrochem. Solid-State Lett.*, **9**, E27 (2006); https://doi.org/10.1149/1.2256688
22. C. Kim, B. Lee, Y. Park, B. Park, J. Lee and H. Kim, *Appl. Phys. Lett.*, **91**, 113101 (2007); https://doi.org/10.1063/1.2783035
23. H.-C. Liu, W.-H. Ho, C.-F. Li and S.-K. Yen, *J. Electrochem. Soc.*, **155**, E178 (2008); https://doi.org/10.1149/1.2988061
24. A. Kahoul and A. Hammouche, *Ionics*, **16**, 105 (2010); https://doi.org/10.1007/s11581-009-0371-z
25. C.S. Tiwary, R. Sarkar, P. Kumbhakar and A.K. Mitra, *Phys. Lett. A*, **372**, 5825 (2008); https://doi.org/10.1016/j.physleta.2008.07.036
26. A.R. Stokes and A.J.C. Wilson, *Proc. Phys. Soc.*, **56**, 174 (1944); https://doi.org/10.1088/0959-5309/56/3/303
27. S.K. Khaja Muswareen and S. Cole, *J. Electron. Mater.*, **50**, 1686 (2021); https://doi.org/10.1007/s11664-020-08534-8
28. S. Jandl and J. Deslandes, *Phys. Rev. B Condens. Matter*, **24**, 1040 (1981); https://doi.org/10.1103/PhysRevB.24.1040
29. A. Mannan, K.R. Kazmi, M.S. Khan and I.H. Khan, *Pak. J. Sci. Ind. Res.*, **49**, 72 (2006).
30. I. Vydrina, A. Malkov, K. Vashukova, I. Tyshkunova, L. Mayer, A. Faleva, S. Shestakov, E. Novozhilov and D. Chukhchin, *Carbohydr. Polym. Technol. Appl.*, **5**, 100305 (2023); https://doi.org/10.1016/j.carpta.2023.100305
31. D. Yadav and R. Shukla, *Optik*, **299**, 171589 (2024); https://doi.org/10.1016/j.ijleo.2023.171589
32. D. Sathya Raj, R. Jayaprakash, T. Prakash, S. kumar, G. Neri and T. Krishnakumar, *Appl. Surf. Sci.*, **266**, 268 (2013); https://doi.org/10.1016/j.apsusc.2012.12.009
33. T. Prakash, T. Arunkumar, D. Sathya Raj and R. Jayaprakash, *Phys. Procedia*, **49**, 36 (2013); https://doi.org/10.1016/j.phpro.2013.10.008
34. M. Arfan, D.N. Siddiqui, T. Shahid, Z. Iqbal, Y. Majeed, I. Akram, Noreen, R. Bagheri, Z. Song and A. Zeb, *Results Phys.*, **13**, 102187 (2019); https://doi.org/10.1016/j.rinp.2019.102187
35. H. Ali and E.S. Mansor, *Colloid Interface Sci. Commun.*, **39**, 100330 (2020); https://doi.org/10.1016/j.colcom.2020.100330